Desorption of Carbon Dioxide from Supersaturated Water in an Agitated Vessel

The rates of desorption of carbon dioxide from supersaturated water solutions into pure carbon dioxide or nitrogen gas stream were measured at 15, 25, and 35°C in a baffled agitated vessel with a flat gas-liquid interface operated in a continuous manner. The volumetric liquid-phase mass transfer coefficients for the bubbles generated in the agitated liquid and the enhancement factors of the volumetric liquid-phase mass transfer coefficient for the free liquid surface due to the bubbling were calculated from the measured desorption rates and correlated as functions of the relative supersaturation of the solution and the liquid-phase Reynolds number.

HARUO HIKITA and YASUHIRO KONISHI

Department of Chemical Engineering
University of Osaka Prefecture Sakai,
Osaka, Japan

SCOPE

Bubbling desorption, that is, gas desorption accompanied by bubble evolution is caused by gas supersaturation of the liquid phase resulting from depressurization, rise in temperature, or chemical reaction. The bubbling desorption process is widely employed in diverse areas of industry such as dissolved air flotation (Takahashi et al., 1979; Rees et al., 1980), coal pyrolysis (Attar, 1978), decarbonization and vacuum degassing in metallurgy processes (Szekely and Martins, 1969; Kinsman et al., 1969), regeneration of spent absorbents in gas purification processes, chemical absorption accompanied by formation of volatile reaction products.

When gas desorption is accompanied by bubble generation, this desorption process is no longer a reverse process of gas absorption. In this case, the area of surface available for mass transfer is determined by external factors and not by the process itself (Danckwerts, 1970). There appears to be no quantitative theory of bubbling desorption.

The purpose of the study is to present the experimental data on the desorption rate of carbon dioxide from supersaturated water solutions under agitated liquid conditions. It is to clarify the mechanism of bubbling desorption, and to determine the effects of the degree of supersaturation of the solution, liquid-phase stirring speed, and liquid temperature on the desorption rate.

CONCLUSIONS AND SIGNIFICANCE

Experiments have been carried out on the bubbling desorption of carbon dioxide from supersaturated water solutions into pure carbon dioxide or nitrogen gas stream using a baffled agitated vessel with a flat gas-liquid interface operated in a continuous manner. The measured desorption rate was divided into the contributions of the interface of the bubbles generated in the agitated liquid and of the free surface of the liquid, from which the volumetric liquid-phase mass transfer coefficient for the bubbles and the enhancement factor of the volumetric liquid-phase mass transfer coefficient for the free surface due to the bubbling were calculated. The existence of two distinctly different regions, low bubbling region and high bubbling region, was found in the investigation of the bubbling desorption rate. The values of the volumetric coefficient for the bubbles and the enhancement factor calculated for each region were correlated as functions of the relative supersaturation of the solution and the liquid-phase Reynolds number.

The experimental results obtained in this work may be a very useful information for the various types of mass transfer operation accompanied by bubble evolution, especially for the chemical absorption processes with bubbling desorption of volatile reaction products.

PREVIOUS WORK

Schweitzer and Szebehely (1950) have measured the absorption and desorption rates of air in various liquids using a shaking cylindrical container. They noted that the desorption process was 0.2 to 10 times quicker than the absorption process owing to the bubble formation. Burrows and Preece (1954) have carried out the experiments on the desorption of air or helium from quiescent supersaturated liquids and presented the empirical equation giving the rate of bubbling desorption. These investigators have also showed that at relative supersaturations as high as 2 or 3.75, bubbling could be prevented under quiescent liquid conditions if the system pressure was reduced gradually. Kamei et al. (1953) have studied the desorption of carbon dioxide from quiescent supersaturated water solutions and presented the empirical formula for the bubbling desorption rate.

Thuy and Weiland (1976) and Weiland et al. (1977) have investigated the desorption of carbon dioxide from supersaturated water solutions under agitated liquid conditions using a multiple-sphere column and a baffled agitated vessel. They found that bubbling always occurred when the partial pressure of the dissolved carbon dioxide exceeded the system pressure and showed that the desorption rate of carbon dioxide increased rapidly with increasing relative supersaturation. Recently Pasiuk-Bronikowska and Rudzinski (1981) have applied the population balance approach to the bubbling desorption of nitrogen produced by the reaction between sulfamic acid and nitrite in aqueous solutions under agitated liquid conditions.

Correspondence concerning this paper should be addressed to Haruo Hikita.

TABLE 1. EXPERIMENTAL CONDITIONS AND PHYSICAL PROPERTIES OF SYSTEMS USED

Bulk Conc. of CO_2, C, mol/m^3	Interfacial Conc. of CO_2, C_f, mol/m^3	Saturated Conc. of CO_2, C_s, mol/m^3	Liquid Temp., t_L, °C	Liquid Stirring Speed, n_L, s^{-1}	$k_{Lf}^* a_f^*$ × 10^4, s^{-1}
51.4–79.1	0.335–1.84	44.7	15	1.00	0.632
47.4–66.2	0.207–1.15	44.7	15	3.33	1.47
35.8–56.8	0.078–0.806	32.8	25	1.00	0.830
35.6–58.9	0.103–1.93	32.8	25	1.67	1.19
35.4–53.2	0.167–0.896	32.8	25	3.33	1.93
34.6–53.7	0.207–1.22	32.8	25	5.00	2.56
28.6–42.4	0.072–0.512	25.1	35	1.00	1.06
27.1–38.3	0.137–0.572	25.1	35	3.33	2.46

EXPERIMENTAL

Apparatus

A schematic diagram of the experimental apparatus is shown in Figure 1. The main parts of the apparatus are a baffled agitated vessel which was used as a carbon dioxide desorber and a carbon dioxide dissolver which was used for preparing water supersaturated with carbon dioxide.

The carbon dioxide dissolver was a 0.09 m^3 steel vessel lined with epoxy resin and was equipped with a perforated-plate gas sparger. The agitated vessel, made of glass, was 12.3 cm I.D. and 20.0 cm in height and was of similar design to that used in the previous work (Hikita et al., 1975). Four equally-spaced vertical baffles, each one twelfth of the vessel diameter in width, were attached to the internal wall of the vessel. The liquid stirrer was a glass paddle agitator with two flat blades, of diameter and height 5.0 cm and 1.5 cm, respectively, and was placed at half of the liquid depth. The liquid level in the vessel was kept equal to the vessel diameter. The gas stirrer was an acryl resin turbine agitator with six flat blades, whose diameter and height were 8.0 cm and 2.0 cm, respectively, and was placed in the center of the gas phase in the vessel. The liquid stirrer was driven at four constant speeds of 1.00, 1.67, 3.33, and 5.00 s^{-1}, and the stirring speed of the gas stirrer was 9.17 s^{-1}. The agitated vessel was operated in a continuous manner with respect to both the gas and liquid. All the desorption experiments were carried out at atmospheric pressure and at 15, 25, and 35°C.

Procedure

Before an experimental run was begun, distilled water of about 0.07 m^3 whose temperature was adjusted to the desired value was introduced into the carbon dioxide dissolver and then pure carbon dioxide taken from a cylinder was bubbled into water through a perforated-plate gas sparger for about 1.5 hours. The total pressure in the dissolver was maintained at a desired constant value in the pressure range of 1.2×10^5 to 5.8×10^5 Pa by adjusting the regulating valve on the carbon dioxide cylinder and the exit valve on the dissolver.

After the flow of carbon dioxide was stopped, the water saturated with carbon dioxide at the given temperature and pressure was continuously fed into the agitated vessel through a capillary which was used to prevent the abrupt drop in static pressure of the water and the subsequent bubble evolution. The flow rate of supersaturated water was held at a desired constant value in the range of 1.9×10^{-6} to 0.43×10^{-6} m^3/s.

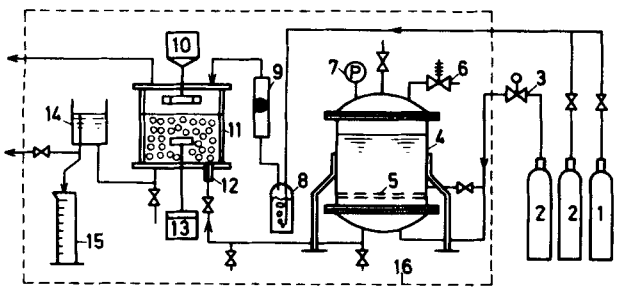

Figure 1. Experimental apparatus: (1) nitrogen cylinder, (2) carbon dioxide cylinder, (3) pressure regulating valve, (4) carbon dioxide dissolver, (5) perforated-plate gas sparger, (6) safety valve, (7) pressure gauge, (8) water vapor saturator, (9) gas flow meter, (10) constant speed motor, (11) carbon dioxide desorber, (12) capillary, (13) variable speed motor, (14) constant head device, (15) measuring cylinder, (16) air bath.

When the agitated vessel had been filled with the water up to a level equal to its diameter, a carrier gas (pure carbon dioxide or pure nitrogen) taken from a cylinder was passed into the agitated vessel through a water vapor saturator and a gas flowmeter. The flow rate of nitrogen ranged from 6.3×10^{-5} to 4.4×10^{-5} m^3/s, while the flow rate of carbon dioxide was kept constant at about 8.5×10^{-6} m^3/s. When nitrogen was used as a carrier gas, the carbon dioxide content in the exit gas stream was calculated from the gas flow rate and the measured desorption rate of carbon dioxide from supersaturated water.

After the gas and liquid were fed into the agitated vessel, both the gas and liquid stirrers were started. The agitated vessel was run for about 40 minutes, after which samples of inlet and exit liquids were taken into a known amount of sodium hydroxide solution. The carbon dioxide concentration in the liquid sample was determined by precipitating the carbon dioxide as barium carbonate using a mixture of barium chloride and standard sodium hydroxide solution. The excess sodium hydroxide was then titrated with hydrochloric acid to a phenolphthalein end point.

The desorption rate of carbon dioxide was calculated from the water flow rate and the difference in carbon dioxide concentrations in the inlet and outlet streams.

The experimental conditions are given in Table 1.

RESULTS AND DISCUSSION

Physical Properties

The physical properties of water supersaturated with carbon dioxide were assumed to be the same as those of pure water, because the content of the dissolved carbon dioxide in the supersaturated water was very low.

The values of the liquid-phase mass transfer coefficient k_{Lf}^* for desorption of carbon dioxide from the free surface in a baffled agitated vessel under nonbubbling conditions were predicted from the following empirical equation which was obtained in the previous work (Hikita et al., 1975):

$$Sh = 0.322 Re^{0.7} Sc^{1/3} \tag{1}$$

where Sh, Re and Sc are the liquid-phase Sherwood, Reynolds and Schmidt numbers, respectively, and are defined as follows:

$$Sh = k_{Lf}^* l / D_A \tag{2}$$

$$Re = d_L^2 n_L \rho_L / \mu_L \tag{3}$$

$$Sc = \mu_L / \rho_L D_A \tag{4}$$

where l is the vessel diameter, D_A is the liquid-phase diffusivity of carbon dioxide, d_L is the diameter of the liquid stirrer, n_L is the liquid-phase stirring speed, and ρ_L and μ_L are the density and viscosity of the liquid, respectively.

The effective interfacial area a_f^* under nonbubbling conditions was assumed to be the same as the geometric interfacial area and was taken to be equal to 8.13 m^{-1}.

The liquid-phase diffusivity D_A of carbon dioxide in water at various temperatures was predicted from the value of 1.97×10^{-9} m^2/s, measured at 25°C (Peaceman, 1951), by correcting for the temperature and viscosity of water according to the well-known Stokes-Einstein relation.

The carbon dioxide concentration C_f at the free liquid surface

was obtained from the bulk partial pressure of carbon dioxide in gas phase and the Henry's law constant for the carbon dioxide–water system, neglecting the gas-phase resistance to mass transfer. The gas-phase resistance was calculated by using the empirical formula obtained in the previous work (Hikita et al., 1975) and was found to be less than 0.23% of the total resistance. The Henry's law constant H_A at 15, 25, and 35°C were tken as 2,230, 2,990, and 3,810 Pa·m^3/mol (Linke and Seidell, 1958).

The saturated concentration C_s of carbon dioxide was estimated from the Henry's law constant described above and the partial pressure of carbon dioxide obtained by subtracting the vapor pressure of water from atmospheric pressure.

The predicted values of the physical properties for the present system are also listed in Table 1.

Results

From visual observations, it seems that the number of generated bubbles depends strongly on the supersaturation of the solution ($C - C_s$), i.e., the concentration driving force for the desorption rate, and the liquid-phase stirring speed n_L, but the diameter of bubbles is almost independent of these parameters. The bubble diameter was found to be up to 1 mm.

The experimental results obtained at 25°C for the case where pure carbon dioxide was used as a carrier gas are shown in Figure 2, where the measured values of the desorption rate N_A of carbon dioxide are plotted on logarithmic coordinates against the supersaturation ($C - C_s$). The dashed lines in this figure show the desorption rate of carbon dioxide under nonbubbling conditions, estimated by using Eq. 1 with $a_f^* = 8.13$ m^{-1}.

The carbon dioxide desorption rate depends considerably on the supersaturation and the liquid-phase stirring speed, Figure 2, but it is independent of the liquid flow rate F in the range of liquid flow rate covered in this work, indicating that the liquid in the agitated vessel is completely mixed. It is also seen that the values of desorption rate under bubbling conditions deviate upward from the desorption rate under nonbubbling conditions represented by dashed lines, particularly at the higher values of the supersaturation ($C - C_s$). The desorption rate N_A varies as the 1.4 power and 3.2 power of the supersaturation ($C - C_s$) at lower and higher values of ($C - C_s$), respectively.

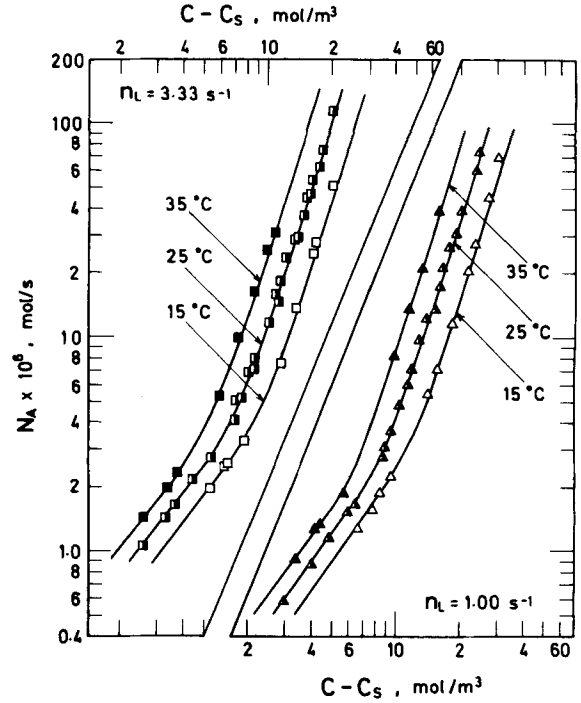

Figure 3. Desorption rate of carbon dioxide into carbon dioxide stream at n_L = 1.00 and 3.33 s^{-1} (effect of liquid temperature).

In Figure 3 the values of the desorption rate N_A obtained at 15 and 35°C are shown. It can be seen that the dependence of desorption rate on the supersaturation observed at 15 and 35°C is the same as that observed at 25°C (Figure 2). Figure 3 also shows that the desorption rate increases with increasing liquid temperature t_L. This increase in the desorption rate may be attributed mainly to the difference in the saturated concentration C_s of carbon dioxide and the physical properties of the supersaturated water.

Figure 4 compares the carbon dioxide desorption rates N_A' obtained for the case where nitrogen was used as a carrier gas with the dashed line representing the desorption rates N_A obtained for

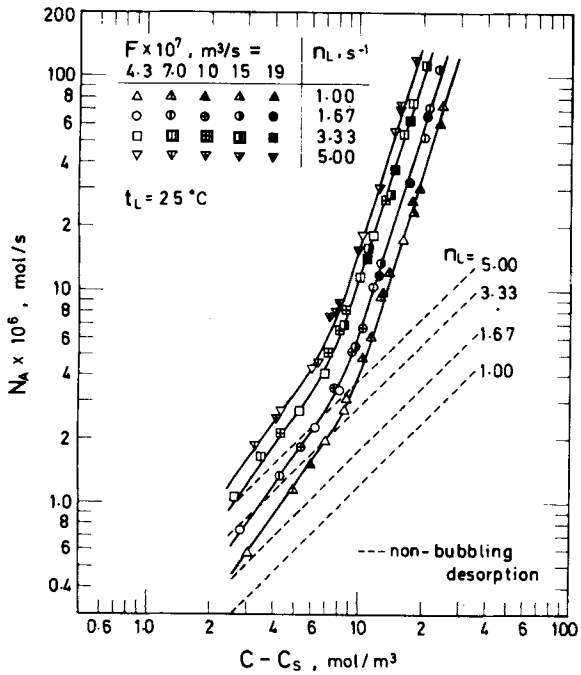

Figure 2. Desorption rate of carbon dioxide into carbon dioxide stream at 25°C (effects of liquid flow rate and liquid-phase stirring speed).

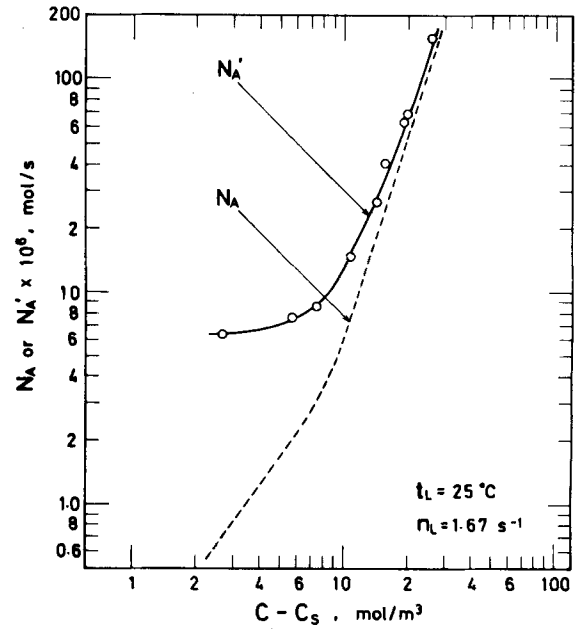

Figure 4. Desorption rate of carbon dioxide into nitrogen stream at 25°C and n_L = 1.67 s^{-1} (comparison with desorption rate into carbon dioxide stream).

the case where carbon dioxide was used as a carrier gas. It can be seen that the desorption rate N'_A of carbon dioxide into nitrogen stream is always higher than the desorption rate N_A into carbon dioxide, but the difference between the two desorption rates roughly remains constant.

Calculation of Volumetric Liquid-Phase Mass Transfer Coefficients

The desorption rate of carbon dioxide measured in the agitated vessel under bubbling conditions may be divided into the contributions of the free surface of the liquid and of the interface of the bubbles generated in the liquid. The desorption from the free surface of the agitated liquid would be the rate-determining step at lower values of the supersaturation, while the desorption from the interface of the generated bubbles controls the rate at higher values of the supersaturation. The experimental results, Figure 4, may be explained reasonably by the mechanism assumed above.

When nitrogen is used as a carrier gas, the desorption rate N'_A of carbon dioxide can be expressed as

$$N'_A = k_{Lf}a_f V(C - C_f) + k_{Lb}a_b V(C - C_s) \tag{5}$$

where $k_{Lf}a_f$ and $k_{Lb}a_b$ are the volumetric liquid-phase mass transfer coefficients under bubbling conditions for the free surface and for the bubbles, respectively; V is the total volume of the liquid in the vessel; C_s is the saturated concentration of carbon dioxide; and C and C_f are the carbon dioxide concentrations in the bulk of the liquid and at the free surface of the liquid, respectively. When carbon dioxide is used as a carrier gas, C_f is equal to C_s and the desorption rate N_A is given by

$$N_A = k_{Lf}a_f V(C - C_s) + k_{Lb}a_b V(C - C_s) \tag{6}$$

Therefore, the values of $k_{Lf}a_f$ and $k_{Lb}a_b$ can be determined from both the desorption rates of carbon dioxide into carbon dioxide and into nitrogen, N_A and N'_A, measured under conditions where the liquid-phase stirring speed, the liquid temperature and the carbon dioxide concentration in the bulk liquid are kept the same.

$$k_{Lf}a_f = \frac{N'_A - N_A}{V(C_s - C_f)} \tag{7}$$

$$k_{Lb}a_b = \frac{N_A}{V(C - C_s)} - \frac{N'_A - N_A}{V(C_s - C_f)} \tag{8}$$

In the present work, the dimensionless quantity ϕ rather than $k_{Lf}a_f$ was used for correlating the data on the desorption from the free liquid surface. The quantity ϕ is the enhancement factor by which the bubbling in the agitated liquid increases the desorption rate compared to the desorption rate under nonbubbling conditions, and is defined by

$$\phi = k_{Lf}a_f / k^*_{Lf}a^*_f \tag{9}$$

where $k^*_{Lf}a^*_f$ is the volumetric mass transfer coefficient for the free liquid surface under nonbubbling conditions.

Correlation for $k_{Lb}a_b$

Supersaturation of the solution is a concentration driving force not only for the bubbling desorption rate studied in this work but also for the crystal nucleation and growth rates in crystallization processes. In the field of crystallization, the relative supersaturation σ which is defined as

$$\sigma = (C - C_s)/C_s \tag{10}$$

is sometimes used for correlating the crystal nucleation and growth rates in preference to the supersaturation $(C - C_s)$, since the temperature effect on the saturated concentration C_s is corrected for. In the present study, the relative supersaturation σ was used to correlate the volumetric mass transfer coefficient $k_{Lb}a_b$ for the bubbles.

In Figure 5 the values of $k_{Lb}a_b$ calculated by the method described above are plotted on logarithmic coordinates against the relative supersaturation σ with the liquid-phase Reynolds number Re as parameter. Data points for each of the Re values fall on straight lines with two different slopes, indicating that there exists two separate regions with respect to effect of the relative supersaturation. At lower σ values, i.e., in the low bubbling region, $k_{Lb}a_b$ is proportional to $\sigma^{0.78}$, while at higher σ values, i.e., in the high bubbling region, $k_{Lb}a_b$ varies as $\sigma^{2.5}$. The vertical difference among the lines in Figure 5 may be due to the difference in the value of Re. In Figure 6 the values of $k_{Lb}a_b$ read from Figure 5 at two σ values of 0.15 and 0.40 are plotted against Re on logarithmic coordinates. The data points for $\sigma = 0.15$ and $\sigma = 0.40$ fall on straight lines with slopes of 0.50 and 0.93, respectively. This indicates that $k_{Lb}a_b$ is proportional to $Re^{0.50}$ in the low bubbling region and to $Re^{0.93}$ in the high bubbling region.

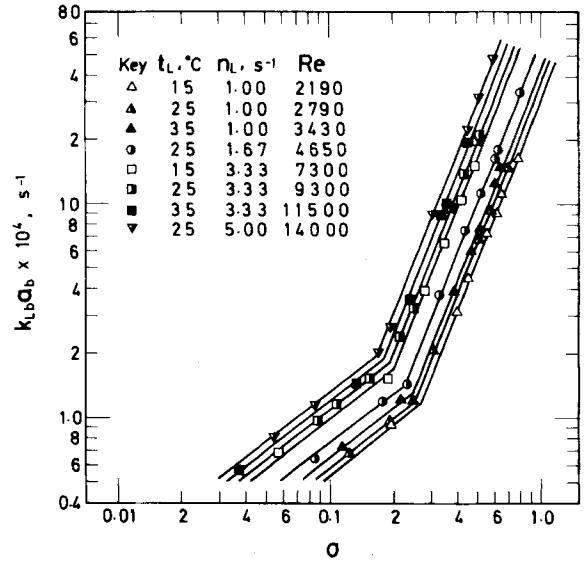

Figure 5. Volumetric coefficient $k_{Lb}a_b$ at several liquid temperatures and liquid-phase stirring speeds as a function of relative supersaturation.

From the results described above, the following equations correlating the volumetric mass transfer coefficient $k_{Lb}a_b$ for the bubbles were obtained:

For the low bubbling region ($\sigma < \sigma_c$)

$$k_{Lb}a_b = 6.77 \times 10^{-6} Re^{0.50} \sigma^{0.78} \tag{11}$$

and for the high bubbling region ($\sigma > \sigma_c$)

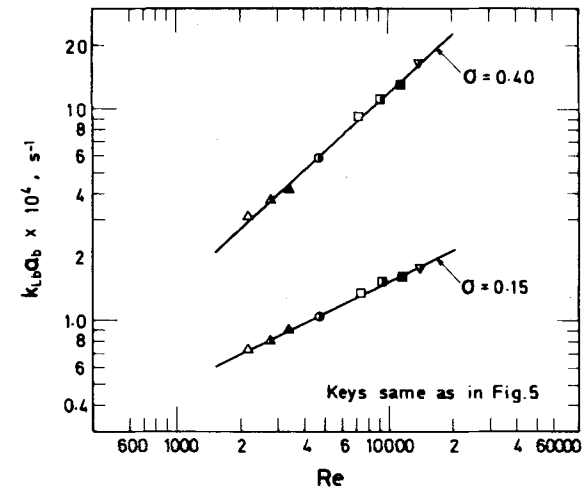

Figure 6. Effect of liquid-phase Reynolds number on volumetric coefficient $k_{Lb}a_b$ at $\sigma = 0.15$ and 0.40.

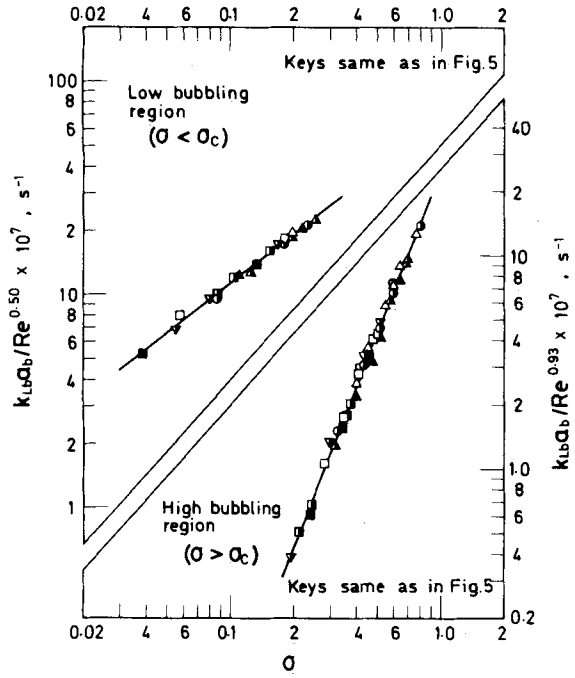

Figure 7. Empirical correlation of volumetric coefficient $k_{Lb}a_b$ in low and high bubbling regions.

$$k_{Lb}a_b = 2.45 \times 10^{-6} Re^{0.93} \sigma^{2.5} \tag{12}$$

where σ_c is the value of σ at intersection of Eqs. 11 and 12 and is given by

$$\sigma_c = 1.81 Re^{-0.25} \tag{13}$$

The ranges of Re and σ over which Eqs. 11 to 13 are valid are as follows:

$$2{,}190 < Re < 14{,}000$$

$$0.038 < \sigma < 0.80$$

Figure 7 presents all the values of $k_{Lb}a_b$ as log-log plots of $k_{Lb}a_b/Re^{0.50}$ vs. σ and of $k_{Lb}a_b/Re^{0.93}$ vs. σ and compares with Eqs. 11 and 12, respectively. The experimental data are in good agreement with Eqs. 11 and 12 with an average deviation of 2.9% and a maximum deviation of 11.0%.

Correlation for ϕ

The values of the enhancement factor ϕ by which the volumetric mass transfer coefficient $k_{Lf}a_f$ for the free liquid surface is increased by the bubbling in the agitated liquid were calculated by using the method described above and were correlated in terms of the relative supersaturation σ of the solution and the liquid-phase Reynolds number Re.

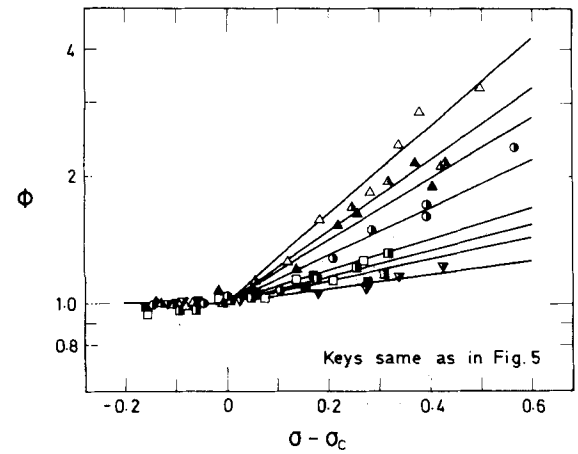

Figure 8. Enhancement factor ϕ at several liquid temperatures and liquid-phase stirring speeds as a function of $(\sigma - \sigma_c)$.

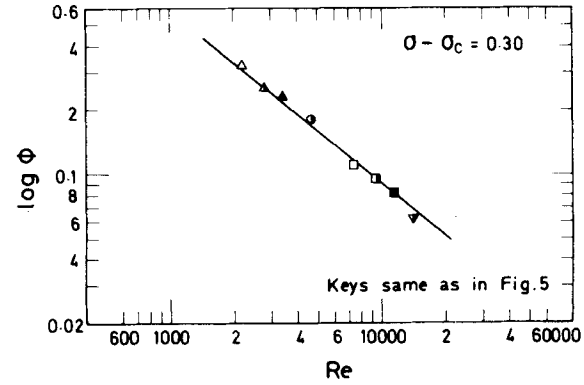

Figure 9. Effect of liquid-phase Reynolds number on enhancement factor ϕ at $(\sigma - \sigma_c) = 0.30$.

In Figure 8 all the values of ϕ are plotted on semilogarithmic coordinates against the value of $(\sigma - \sigma_c)$. The effects of σ and Re on ϕ in the low bubbling region are very much different from those in the high bubbling region. When the σ value is less than σ_c, i.e., in the low bubbling region, the value of ϕ is independent of both σ and Re and practically shows unity, indicating that the enhancement effect of bubbling on the $k_{Lf}a_f$ value can be neglected. On the other hand, when the σ value is greater than σ_c, i.e., in the high bubbling region, the data points representing the ϕ values for each of the Re values fall on a straight line, indicating that $\log\phi$ is proportional to $(\sigma - \sigma_c)$, and its slope increases with decreasing Re. Figure 9 is a log-log plot of the logarithmic values of ϕ read from Figure 8 at a constant $(\sigma - \sigma_c)$ value of 0.30 vs. Re. The data points can be represented by a straight line with a slope of -0.81. This indicates that $\log\phi$ is proportional to $Re^{-0.81}$.

From the results described above, the following equations correlating the enhancement factor ϕ of the volumetric mass transfer coefficient for the free liquid surface due to the bubbling were obtained:

For the low bubbling region $(\sigma < \sigma_c)$

$$\phi = 1 \tag{14}$$

and for the high bubbling region $(\sigma > \sigma_c)$

$$\log\phi = 522(\sigma - \sigma_c) Re^{-0.81} \tag{15}$$

The ranges of σ and Re over which Eqs. 14 and 15 are valid are the same as those for Eqs. 11 and 12.

Figure 10 presents all the values of ϕ as a semilogarithmic plot

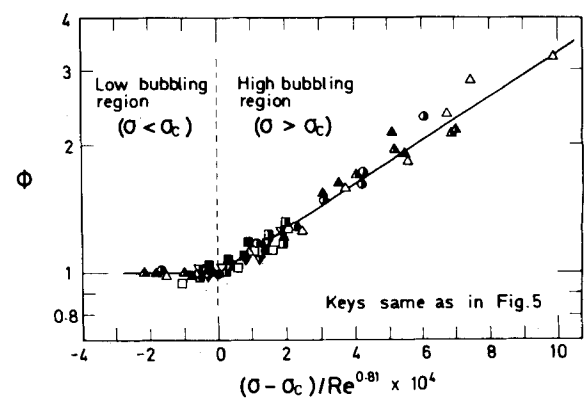

Figure 10. Empirical correlation of enhancement factor ϕ in low and high bubbling regions.

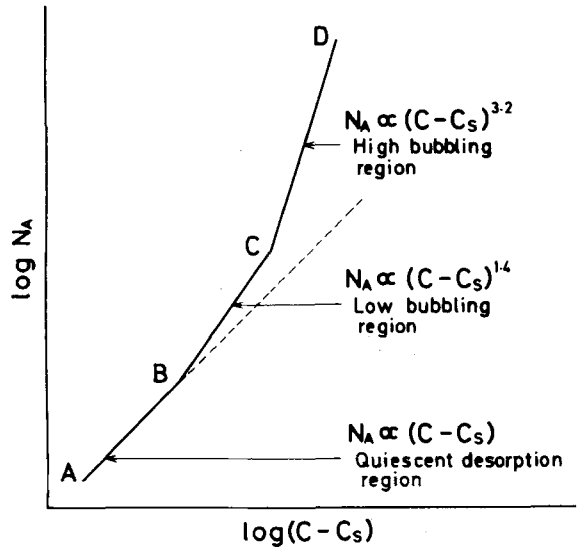

Figure 11. Variation of carbon dioxide desorption rate into carbon dioxide stream with concentration driving force.

of ϕ vs. $(\sigma - \sigma_c)Re^{-0.81}$ and compares with Eqs. 14 and 15. The experimental data are in good agreement with Eqs. 14 and 15 with an average deviation of 3.4% and a maximum deviation of 18.0%.

Discussion

From the experimental results obtained in the present work it is evident that the supersaturation of the solution is an important factor for determining the bubbling desorption rate. We will now discuss the effect of supersaturation or concentration driving force on the carbon dioxide desorption rate from supersaturated water in an agitated vessel into carbon dioxide stream.

Figure 11 shows qualitatively the dependence of the carbon dioxide desorption rate on the concentration driving force as a log-log plot of N_A vs. $(C - C_s)$. There exists three different regions with respect to effect of $(C - C_s)$. In the range AB, designated as the quiescent desorption region, no bubbles are generated and desorption occurs by molecular diffusion across the free liquid surface. As might be expected from this mechanism, N_A is proportional to the concentration driving force $(C - C_s)$. In the range above point B, called the bubbling desorption region, bubbling occurs and it enhances the desorption rate. This bubbling desorption region is divided into two separate regions, BC and CD. In the range BC, designated as the low bubbling region, mild bubbling takes place and N_A varies as the 1.4 power of the driving force $(C - C_s)$. The increase in the desorption rate N_A due to the bubbling in this case is not very much and the N_A value is less than 2.8 times that under quiescent desorption conditions. The transition from quiescent to bubbling desorption region, represented by point B, occurs when the bulk concentration C is nearly equal to the saturated concentration C_s, i.e., when $(C - C_s)$ is very small, as pointed out by Thuy and Weiland (1976) and by Weiland et al. (1977). In the range CD, designted as the high bubbling region, vigorous bubbling takes place and N_A is proportional to the 3.2 power of $(C - C_s)$. The desorption rate in this region is greatly enhanced by the bubble generation and the subsequent turbulence and goes up to 31 times that under quiescent desorption conditions. The transition from low to high bubbling region, represented by point C, occurs at the value of $(C - C_s)$ calculated from Eq. 13.

It should be noted that the effect of the driving force on the transfer rate in the bubbling desorption process is analogous to that in the crystallization and nucleate boiling processes. According to Mersmann (1979), the crystal nucleation rate is proportional to the 3 to 6 power of the supersaturation, i.e., the concentration driving force. McAdams (1954) described that in the nucleate boiling region the heat transfer rate increases as the 3 to 4 power of the temperature driving force, i.e., the temperature difference between the temperature of the heating surface and the saturated temperature of the liquid. These power law relationships between the transfer rate and the driving force may be considered to be a specific characteristic of the transport phenomena accompanied by bubble or crystal nucleation.

NOTATION

a_f^* = effective interfacial area for free surface under nonbubbling conditions, m^{-1}
C = concentration of carbon dioxide in bulk liquid, mol/m^3
C_f = concentration of carbon dioxide at free liquid surface, mol/m^3
C_s = saturated concentration of carbon dioxide, mol/m^3
d_L = diameter of liquid stirrer, m
D_A = liquid-phase diffusivity of carbon dioxide, m^2/s
F = volumetric flow rate of liquid, m^3/s
H_A = Henry's law constant for carbon dioxide in water, Pa·m^3/mol
$k_{Lb}a_b$ = volumetric liquid-phase mass transfer coefficient for bubbles, s^{-1}
$k_{Lf}a_f$ = volumetric liquid-phase mass transfer coefficient for free liquid surface, s^{-1}
k_{Lf}^* = liquid-phase mass transfer coefficient for free liquid surface under nonbubbling conditions, m/s
l = diameter of agitated vessel, m
n_L = liquid-phase stirring speed, s^{-1}
N_A = desorption rate of carbon dioxide into carbon dioxide stream, mol/s
N_A' = desorption rate of carbon dioxide into nitrogen stream, mol/s
Re = liquid-phase Reynolds number, $d_L^2 n_L \rho_L / \mu_L$
Sc = liquid-phase Schmidt number, $\mu_L / \rho_L D_A$
Sh = liquid-phase Sherwood number, $k_{Lf}^* l / D_A$
t_L = liquid temperature, °C
V = volume of liquid in vessel, m^3

Greek Letters

μ_L = viscosity of liquid, Pa·s
ρ_L = density of liquid, kg/m^3
σ = relative supersaturation, $(C - C_s)/C_s$
σ_c = relative supersaturation at intersection of Eqs. 11 and 12
ϕ = enhancement factor of volumetric liquid-phase mass transfer coefficient for free liquid surface due to bubbling, $k_{Lf}a_f / k_{Lf}^* a_f^*$

LITERATURE CITED

Ang, H-M., and J. W. Mullin, "Crystal Growth Rate Determinations from Desupersaturation Measurements: Nickel Ammonium Sulphate Hexahydrate," *Trans. Inst. Chem. Engrs.*, **57**, 237 (1979).

Attar, A., "Bubble Nucleation in Viscous Material due to Gas Formation by a Chemical Reaction: Application to Coal Pyrolysis," *AIChE J.*, **24**, 106 (1978).

Burrows, G., and F. H. Preece, "The Process of Gas Evolution from Low Vapour Pressure Liquids upon Reduction of Pressure," *Trans. Inst. Chem. Engrs.*, **32**, 99 (1954).

Danckwerts, P. V., *Gas-Liquid Reactions*, 265, McGraw-Hill, New York (1970).

Hikita, H., S. Asai, H. Ishikawa, and Y. Saito, "Kinetics of Absorption of Chlorine in Aqueous Acidic Solutions of Ferrous Chloride," *Chem. Eng. Sci.*, **30**, 607 (1975).

Kamei, S., K. Kimura, S. Hochi, and K. Matsusaka, "Desorption of Carbon Dioxide," *Kagaku Kogaku*, **17**, 309 (1953).

Kinsman, G. J. M., G. S. F. Hazeldean, and M. W. Davies, "Physicochemical Factors Affecting the Vacuum Deoxidation of Steels," *J. Iron Steel Inst.*, **207**, 1463 (1969).

Linke, W. F., and A. Seidell, *Solubilities of Inorganic and Metal-Organic Compounds*, 4th Ed., I, 459, van Nostrand, New York (1958).
McAdams, W. H., *Heat Transmission*, 3d Ed., 370, McGraw-Hill, New York (1954).
Mersmann, A. B., W. F. Beer, and D. Seifert, "Current State of Crystallizer Design," *Ger. Chem. Eng.*, **2**, 1 (1979).
Pasiuk-Bronikowska, W., and K. J. Rudzinski, "Gas Desorption from Liquids," *Chem. Eng. Sci.*, **36**, 1153 (1981).
Peaceman, D. W., "Liquid-Side Resistance in Gas Absorption with and without Chemical Reactions," Sc. D. Thesis, Mass. Inst. Tech., Cambridge (1951).
Rees, A. J., D. J. Rodman, and T. F. Zabel, "Dissolved Air Flotation for Solid/Liquid Separation," *J. Separ. Proc. Technol.*, **1**, 19 (1980).
Schweitzer, P. H., and V. G. Szebehely, "Gas Evolution in Liquids and Cavitation," *J. Appl. Phys.*, **21**, 1218 (1950).
Szekely, J., and G. P. Martins, "Studies in Vacuum Degassing," Part 1, *Trans. Met. Soc. AIME*, **245**, 629 (1969).
Takahashi, T., T. Miyahara, and H. Mochizuki, "Fundamental Study of Bubble Formation in Dissolved Air Presure Flotation," *J. Chem. Eng. Japan*, **12**, 275 (1979).
Thuy, L. T., and R. H. Weiland, "Mechanism of Gas Desorption from Aqueous Solutions," *Ind. Eng. Chem. Fund.*, **15**, 286 (1976).
Weiland, R. H., L. T. Thuy, and A. N. Liveris, "Transition from Bubbling to Quiescent Desorption of Dissolved Gases," *Ind. Eng. Chem. Fund.*, **16**, 332 (1977).

Manuscript received August 31, 1982; revision received August 15, and accepted August 21, 1983.

Theory and Operational Characteristics of the Magnetic Value for Solids

Part I: Grate Design

The operational characteristics of the grate-type MVS with screen were studied in detail. First, theory was developed to predict how the current needed to operate the valve was related to the valve geometry. Then experiments were made to see how bed height, screen aperture, grate spacing, the presence of nonmagnetic solids in the mixture all affected the current needed to operate the valve and on the mass flux of solids. The response time of the valve was also determined.

The experiments were compared with the predictions of the theory.

ELADIO JARAIZ-M., YANG WANG, GUO-TAI ZHANG, and OCTAVE LEVENSPIEL

Chemical Engineering Department
Oregon State University
Corvallis, OR 97331

SCOPE

Magnetism has long been used to separate magnetic solids from nonmagnetic solids and fluids. More recently this technique has been extended to the removal of very weak paramagnetic particles from gas streams, by using high-gradient magnetic filtration. All of this is well known, and these techniques have been well developed. In recent years magnetism has also been used to transform fluidized beds into magnetic stabilized beds which have some interesting properties.

Magnetism can also be used to stop the flow of a dense stream of magnetic particles and by turning the field on and off one can then control the movement of this stream of magnetic particles and thus approach any desired contacting pattern in a gas/solid reactor.

This new type of valve, called magnetic valve for solids (MVS), presents important advantages over conventional devices for controlling the flow of a stream of flowing particles: (1) it does not use moving parts; (2) it can reliably act as a distributor-downcomer for multistage fluidized beds without the problems of bypassing, plugging, etc., previously mentioned; (3) its time response is practically instantaneous; and (4) it can be used either with pure magnetic particles or with mixtures of magnetic and nonmagnetic solids.

There are three main designs of the MVS: the grate-MVS, the collar-MVS, and the adjacent-MVS. Each one presents some advantages and some disadvantages. This work was undertaken to study the operational characteristics of the grate design. The main objectives of this study are:

(1) To develop a simple theory to explain the functioning of this type of MVS.

(2) To measure its operational characteristics so as to obtain useful information for design and for comparison with other designs to be tested.

E. Jaraiz-M. is on leave from Departamento de Quimica Tecnica, University of Salamanca, Spain; Y. Wang, from The Institute of Coal Chemistry, Chinese Academy of Sciences, Taiyuan, Shanxi, China; and G. Zhang, from East China Institute of Chemical Technology, Shanghai, China.